# How does hydrogen transform into shallow donors in silicon?

Akira Kiyoi[1,*] and Takahide Umeda[2]
[1]*Advanced Technology R&D Center, Mitsubishi Electric Corporation, Amagasaki 661-8661, Japan*
[2]*University of Tsukuba, Tsukuba 305-8573, Japan*

(Received 23 March 2023; accepted 24 October 2023; published 5 December 2023)

We conducted electron paramagnetic resonance (EPR) and cyclotron resonance studies on hydrogen-related donors (HDs) in silicon, whose origins have remained unclear for 50 years. In floating-zone silicon substrates irradiated with 2-MeV protons, followed by optimized annealing at 400 °C and 500 °C, we identified three original EPR spectral signals originating from HDs, labeled the MT1, MT2, and MT3 centers. The three centers exhibited a tetragonal symmetry around the ⟨100⟩ axis and were classified into two types of HDs: a HD with a lower thermal stability and a normal single-donor nature/positive-$U$ nature (MT1), and a HD with a higher thermal stability and a double-donor nature/negative-$U$ nature (MT2 and MT3). Most importantly, the MT2 center revealed $^{29}$Si hyperfine interactions closely resembling the B3 EPR center with a tetragonal symmetry, which has been identified as a tetrainterstitial cluster, $I_4$. Contrarily, we could not resolve any $^1$H hyperfine interactions for the three MT centers. According to the experimental results, an atomistic model was proposed for the HDs based on the $I_4$ center weakly coupled with hydrogen atom(s). We deduce that different numbers of incorporated hydrogen atoms and/or different types of hydrogen bonding to $I_4$ generated the two types of HDs. These findings are the first step in understanding how hydrogen works as a donor in Si and offer important insights into the use of proton-irradiation doping processes in device applications.

DOI: 10.1103/PhysRevB.108.235201

## I. INTRODUCTION

Hydrogen is a chemically active element that interacts with crystalline lattices as well as defects and impurities in a variety of materials. Such interactions can modify the electrical and optical properties of materials, particularly Si. As shown in Fig. 1, hydrogen in Si is typically found in three forms: (a) mobile, (b) bound, and (c) shallow donors, which have been intensively studied by several experimental and theoretical works since the early 1980s [1–9].

The most fundamental configuration of hydrogen in Si is isolated atomic hydrogen [Fig. 1(a)] [5–9]. Previous studies have revealed that $H^+$ is stable at bond-center (BC) sites with a large relaxation of its neighboring Si atoms, and $H^-$ is stable at tetrahedral interstitial sites. Theoretical studies have proposed three different charge states of hydrogen [10,11], where $H^+$ and $H^-$ have the lowest energies in $p$-type and $n$-type Si, respectively, and $H^0$ is unstable at any Fermi level position; this means that the isolated H atom in Si has a negative-$U$ nature [12].

Isolated hydrogen is highly mobile; therefore, it will bond with other hydrogen atoms to form $H_n$ aggregates even at room temperature. The smallest $H_n$ involves two hydrogen atoms ($H_2$ [11] and $H_2^*$ [13]), which have been predicted theoretically and observed using Raman [14] and infrared-absorption spectroscopies [15,16].

Hydrogen also interacts with defects, resulting in the deactivation of the electrical activity of these defects [17,18] or in the formation of new electrically active centers [19–21] [Fig. 1(b)]. Hydrogen-containing defects (e.g., platelets [21] and vacancy-H defects [19]) exhibit a variety of hydrogen bonds, such as Si-H bonds [17–21]. Through the interaction with hydrogen, the formation of a different deep level has been investigated in Si devices [20].

Hydrogen can also lead to the formation of shallow-donor states [hydrogen-related donors (HDs)] [22–25]. This phenomenon has recently given rise to a different doping method in Si devices [26–29]. HDs form via an *unidentified structural unit* that extracts electrons from hydrogens in Si [Fig. 1(c)]. HDs have been observed in neutron [30], electron [31], and proton-irradiation [32–35] experiments when sufficient hydrogen was available in irradiated Si materials. Therefore, unidentified structural units are phenomenologically considered as radiation-induced defects. The microscopic structures of HDs have been discussed based on experimental results and density functional theory (DFT) calculations. A hydrogen- and carbon-incorporated thermal donor [$C_iO_i(n)$−H] [36–38] was demonstrated as a model for HDs. HDs were also reported to be related to intrinsic defects (vacancies and interstitial silicon and their clusters) [23–25,28,29,32–34].

Besides, the microscopic model of unidentified structural units is missing, and the mechanism of generating the donor state from hydrogen atoms has also remained unclear for over half a century. Therefore, understanding HDs remains an important challenge to be addressed in the field of fundamental defect physics for modern silicon device technology.

In this study, we found a "double-donor" nature of the HDs [see Fig. 1(c)] and identified the unidentified structural

*Corresponding author: Kiyoi.Akira@ay.MitsubishiElectric.co.jp

 

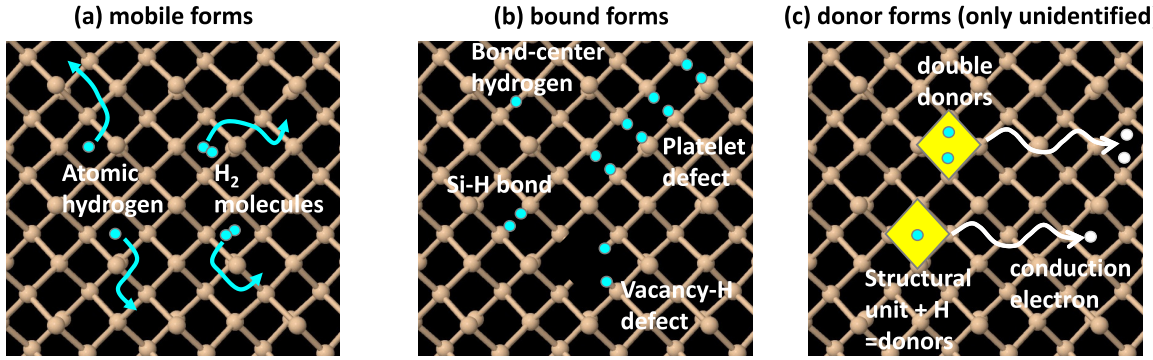


FIG. 1. (a) Mobile (atomic hydrogen and $H_2$ molecules); (b) bound (e.g., Si-H bonds and bond-center form); and (c) shallow-donor state via an unidentified structural unit that extract conduction electrons from hydrogen atoms. The hydrogen and Si atoms are indicated by light blue and orange colors, respectively.

units of HDs. Our electron paramagnetic resonance (EPR) studies identified three types of paramagnetic centers with the following features: (i) tetragonal symmetry around the ⟨100⟩ axis; (ii) one center with negative-$U$ nature, following an exchange-narrowing signal, and hyperfine (HF) interaction with $^{29}$Si nuclear spin, similar to that of a B3 EPR center [39]; and (iii) HF interactions with $^{1}$H nuclear spins were not resolved for all centers. These results afford interesting insights into the atomic structure of the HDs, enabling us to advance the proposition of a suitable microscopic model for HDs based on the $I_4$ center weakly coupled with hydrogen atom(s).

## II. EXPERIMENT

Phosphorus (P)-doped (100) FZ-Si with a high resistivity of ∼ 830 Ω cm was used as the substrate. The wafer was irradiated with 2-MeV protons with a total dose of $5 \times 10^{14}$ cm$^{-2}$ using a cyclotron particle accelerator. Back surface polishing was applied to produce thin samples ($0.3 \times 0.8 \times 0.01$ cm$^3$), which were annealed at 400 °C and 500 °C for 1 h in an ambient air environment. Surface treatments with diluted hydrogen fluoride and tetramethylammonium hydroxide were applied to remove the surface damage layers. Furthermore, two-point spreading resistance (SR) profiles were obtained using a solid-state measurement (SSM-2000) instrument with a bevel angle of 2.5 °.

The EPR and cyclotron resonance (CR) spectra were measured using a Bruker E500 X-band spectrometer with a Bruker ER4122SHQ cavity and an Oxford instruments ESR900 He cryostat. We examined the stacked samples (a set of either 14 or 24 slices) in the cavity. The HF interactions in the EPR spectra were examined using the latter sample set. We performed EPR measurements both in the dark and under photoexcitation (100 W halogen cold lamp). With this illumination condition, the photoexcited changes in the EPR and CR spectra were fully saturated. The EPR and CR measurements were performed with a 100-kHz magnetic field modulation of 0.1- and 0.5-mT widths, respectively. To check the symmetry and spectroscopic nature of the observed signals, we examined their angular dependencies by rotating the magnetic field (**B**) in the $(0\bar{1}1)$ plane. The magnetic field angles of 0° and 90° correspond to **B**//[100] and **B**//[011], respectively. This rotation system is the most conventional one used in previous EPR studies for silicon.

## III. RESULTS

### A. Depth profile of HDs

The proton irradiation and subsequent annealing processes induced deep- and shallow-level defects [20–23]. Figure 2 shows the carrier concentration profiles of the proton-irradiated FZ-Si after annealing treatments. The depth of the projected ion range ($R_p$) from the incident surface was ∼ 44.5 μm, which is in accordance with the stopping and range of ions in matter (SRIM) simulations [40]. $N$-type to $p$-type conversion occurred in the penetrated layers (extending from the surface to the $R_p$ depth) owing to the irradiation-induced shallow acceptor-type defects. The broad peaks of the carrier concentration around the $R_p$ depth correspond to the $n$-type region where shallow HDs were formed because of the interaction between the introduced hydrogen and the irradiation-induced defects after the annealing treatment. Consequently, $p$-$n$ junctions were observed at a depth of 20 μm and near the surface for the samples annealed at 400 °C

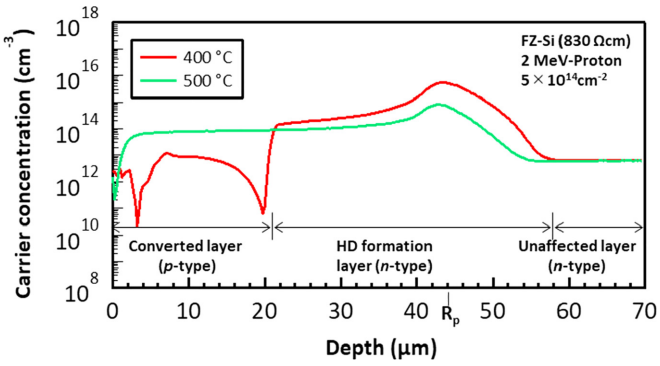


FIG. 2. Carrier concentration profiles of FZ-Si irradiated with 2-MeV protons and subsequently annealed at 400 °C and 500 °C. The profiles were obtained from SR measurements. The conversion to carrier concentration profiles was performed using Thurber's curve [41]. For the profile of the sample annealed at 400 °C (red), the $n$-type to $p$-type converted layer, the layer where HDs were formed, and the unaffected substrate are indicated.

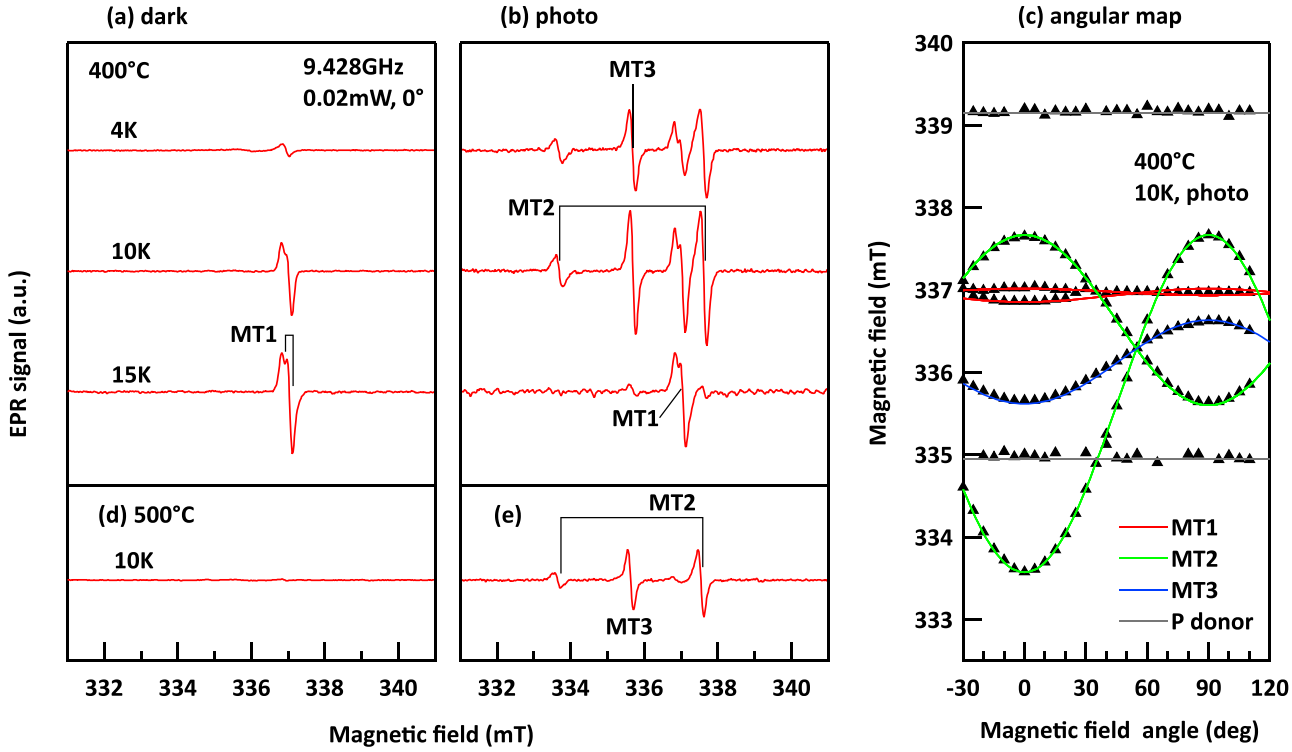


FIG. 3. EPR spectra of HDs in proton-irradiated FZ-Si after 400 °C annealing, measured (a) in the dark and (b) under photoexcitation conditions. All spectrum were measured with a magnetic field parallel to the [100] axis (magnetic field angle = 0°). (c) Angular maps of MT1, MT2, and MT3 at 9.428 GHz. The magnetic field was parallel to the [100] and [011] axes for 0 ° and 90 °, respectively. The symbols indicate the experimental data. Solid lines correspond to the simulation data using the spin-Hamiltonian (SH) parameters given in Table II. The angular map of P donors (included in the base substrate) was also simulated using $g = 1.998\,50$ and $^{31}$P hyperfine-splitting width = 4.195 mT [45]. EPR spectra in proton-irradiated FZ-Si after 500 °C annealing measured (d) in the dark and (e) under photoexcitation.

and 500 °C, respectively. At 58 μm and a deeper range, a base *n*-doping level was observed. In fact, we detected a weak EPR signal of shallow P donors in the substrate.

### B. EPR signals of HDs

Figure 3 shows the low-temperature EPR spectra of the proton-irradiated Si after annealing at 400 °C. Owing to the strong dielectric loss of the free carriers, the spectra were only measurable below 25 K. In the EPR spectra [Figs. 3(a) and 3(b)], three new EPR signals related to the HDs were observed; hereafter, "MT1," "MT2," and "MT3." The MT1 (electron spin, $S = 1/2$) signal appeared in the dark (thermal equilibrium), whereas the MT2 and MT3 (both $S = 1/2$) signals were only observable under photoexcitation at low temperatures (< 15 K). Their angular maps [Fig. 3(c)] formed different patterns compared to those of previously reported EPR centers [42]. We assume that MT2 and MT3 belong to the same defect because MT3 was observed as the averaged signal of MT2. Therefore, the EPR signals related to the HDs could be classified into two different types of dark and photoexcited centers (MT1 and MT2/3, respectively).

For the sample annealed at 500 °C [Figs. 3(d) and 3(e)], only MT2 and MT3 were observed with weaker intensities than those of the 400 °C sample. The total spin concentrations of the MT1, MT2, and MT3 centers are listed in Table I. For both the samples annealed at 400 °C and 500 °C, the total spin concentrations agree well with the total HD concentrations within the experimental errors. Thus, we conclude that the observed EPR centers arise from the HDs. Thus far, two types of HDs have been reported: one (described as "HD1") was found to decay at 380–440 °C and the other ("HD2") at 500–540 °C [34,43,44]. Therefore, we assign that the MT1 center corresponds to HD1 with a lower thermal stability, and the MT2/3 centers are another HD with a higher thermal stability (HD2).

The angular maps [Fig. 3(c)] of the EPR centers reveal the nature of HDs. The solid lines were fitted using the *g* tensor in Table II. The MT1 center was similar to the conduction electron resonance ($g = 1.998\,75$) but was weakly anisotropic; e.g., the MT1 signal weakly split into double peaks when **B** was set to 0° [Figs. 3(a) and 3(b)]. This weak anisotropy is shown in Fig. 4: MT1 splits into double peaks with a 1:2 ratio for 0° or **B**//[100], it sharpens the most for 54.75° or **B**//[111], and finally it broadens slightly for 90° or **B**//[011]. Such features can be reproduced exactly by assuming a tetragonal symmetry (⟨100⟩ axial symmetry) with $g_{//} = 1.999\,70$ and $g_{\perp} = 1.998\,75$ for this center. Furthermore, the determined *g* tensor can completely fit the observed angular dependence of MT1 [see Fig. 3(c)]. The conduction-electron-like *g* value of MT1 indicates that MT1 is a type of shallow-donor electron weakly coupled with a tetragonal-symmetrical point defect.

Contrarily, the MT2 center was found to be strongly anisotropic with the same tetragonal symmetry. The corresponding *g* tensor was given by $g_{//} = 2.019\,38$ and $g_{\perp} =$

TABLE I. Concentrations of the hydrogen-related donors and EPR centers (MT1 and MT2/3) in proton-irradiated FZ-Si after annealing at 400 °C and 500 °C. The donor concentration was calculated by integrating the carrier concentrations shown in Fig. 2. The spin concentration was calculated from an EPR spectrum measured under photoexcitation at 10 K with a magnetic field parallel to the [100] axis. The intensity ratio of MT3 and MT2, "MT3/MT2," was calculated from areas of absorption EPR signals (integrated signals).

| Annealing temperature | Donor concentration ($cm^{-2}$) | Spin concentration (spins/$cm^2$) | | | |
|---|---|---|---|---|---|
| | | Total | MT1 | MT2, MT3 | MT3/MT2 |
| 400 °C | $3.86 \times 10^{12}$ | $3.15 \times 10^{12}$ | $1.30 \times 10^{12}$ | $1.85 \times 10^{12}$ | 0.69 |
| 500 °C | $0.79 \times 10^{12}$ | $0.68 \times 10^{12}$ | undetectable | $0.68 \times 10^{12}$ | 0.66 |

1.994 90. This strong anisotropy implies a large structural distortion in this center along the ⟨100⟩ axis and may be related to its higher thermal stability. The tetragonal symmetry is known for only a few point defects in Si [42]; e.g., the B3 center, identified as the $I_4(+)$ center in Si [39], as noted in Table II.

MT3 was always observed together with MT2 and was detected exactly at the center of two split peaks of MT2 for all angles [Fig. 3(c)]. Therefore, we attribute this signal to an exchange-narrowing signal of the MT2 center. This is supported by the fact that, unlike MT2, MT3 exhibited a single Lorentzian-like peak without any HF structures (see Sec. III D). Feher *et al.* reported similar findings for Si, demonstrating the exchange-narrowing interaction of shallow P donors with $1 \times 10^{18}$ $cm^{-3}$ or higher concentrations when the average distance of P donors was $\leqslant$10 nm [45]. For HD concentrations (peak values $= 8 \times 10^{15}$ $cm^{-3}$ for 400 °C and $1 \times 10^{15}$ $cm^{-3}$ for 500 °C; see Fig. 2), their average separations are estimated to be 50 and 100 nm, respectively, appearing to be much larger than the spatial extent of any shallow donors with exchange-narrowing interactions in Si. Nevertheless, MT3 was detectable in both samples and even with a similar intensity ratio (MT3/MT2 = 0.66–0.69; see Table I).Therefore, we strongly suggest that the formation of close pairs of HD2 is favorable, resulting in the all-time coexistence of the MT2 and MT3 signals.

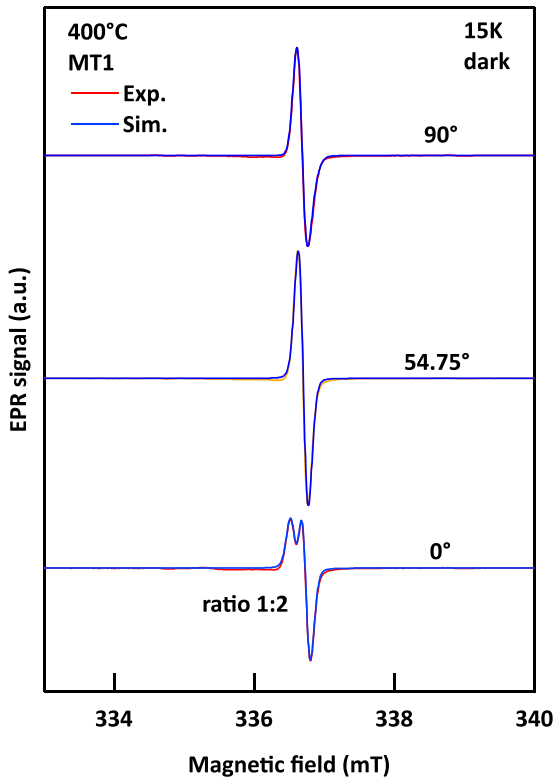


FIG. 4. Angular dependence of the MT1 spectra with tetragonal symmetry. The spectral simulations based on tetragonal symmetry (blue lines) fully reproduced the observed characteristic of the MT1 spectra.

### C. Cyclotron resonance of conduction-band electrons

Comparing the EPR results with CR spectroscopic results described in this section, we further reveal a double-donor nature of the HDs. Figures 5(a) and 5(b) compare the CR spectra in the dark and under photoexcitation, where the conduction-band electrons (CEs) are observable in a very low field range. As far as the CR spectra are concerned, the 400 °C and 500 °C samples were very similar with a slight fluctuation in their temperature dependencies. Below 25 K, we found two broad peaks related to CR [Fig. 5(c)]. We also found a tetragonal symmetry of CEs in association with the ⟨100⟩-oriented ellipsoidal six-valleys of the conduction-band minima in Si [Fig. 5(d)] [46]. The solid lines indicate the simulation data obtained using the known electron effective mass $m^*$ and the electron rest mass $m_0$ for Si (longitudinal and transverse effective masses, $m_l^* = 0.98m_0$ and $m_t^* = 0.19m_0$, respectively [46]). Note that the tetragonal symmetry of the CEs is independent of the tetragonal symmetry of the HDs because the former is always found for any conventional donors such as the P donor (cubic symmetry). The relationship between HDs and CEs can be examined using the CR signals.

At 15 K (and higher temperatures), the CR signal was clearly detectable in the dark [Fig. 5(a)] in *both* samples (400 °C sample: HD1 and HD2; 500 °C sample: only HD2). This indicates that the CEs are emitted from HD2s at 15 K, and HD2 should be stabilized into an empty state ($S = 0$). Previously, in low-temperature *CV* measurements, freeze-out behaviors of HD1 and HD2 were found to obey activation energies of 70–80 meV and 30–40 meV, respectively [34]. Judging from such data, we consider that the HD1s were frozen at 15 K, resulting in the formation of a singly occupied state of the MT1 EPR center. The observed situations and their interpretations are listed in Table III.

When the temperature was decreased to 10 K, the CR signal completely disappeared [Fig. 5(a)], indicating that the CEs were converted into their frozen states with the HDs. Nevertheless, HD2 did not show its EPR signal and kept an $S = 0$ state. Namely, each HD2 received *double* electrons and

TABLE II. SH parameters of the EPR centers of the HDs, MT1, MT2, and MT3. The conditions indicate the typical observation conditions for each center, under which the SH parameters were determined. For each center, SH was defined as $H = \mu_B \mathbf{B} \cdot \mathbf{g} \cdot \mathbf{S} + \Sigma_i \mathbf{I}_i \cdot \mathbf{A}_i \cdot \mathbf{S}$ [39], where $\mu_B$ is the Bohr magneton, $\mathbf{B}$ is the external magnetic field, $\mathbf{g}$ is the $g$ tensor, $\mathbf{S}$ is the spin operator, $\mathbf{I}_i$ is the $^{29}$Si nuclear spin operator ($i$ is its suffix), and $\mathbf{A}_i$ is the HF tensor for each nuclear spin. Only the MT2 center revealed resolved $^{29}$Si HF structures that resembled those of the B3 ($I_4$) center [39]. $N$ is the number of Si atoms included in the first to third shells [39]. Within tetragonal symmetry, the symmetry axes of $\mathbf{g}$ and $\mathbf{A}_i$ (principal $g_{//}$ and $A_{//}$ axes) are given by a ⟨100⟩ axis.

| Center | Spin | | $g$ tensor ($\mathbf{g}$) | | $^{29}$Si HF tensor ($\mathbf{A}_i$) | | | | Reference |
|---|---|---|---|---|---|---|---|---|---|
| (condition) | $S$ | Symmetry | $g_{//}$ | $g_\perp$ | Shell | $N$ | $A_{//}$ (mT) | $A_\perp$ (mT) | defect model |
| MT1 (dark and photo, 10 K) | 1/2 | tetragonal | 1.999 70 | 1.998 75 | not observed | | | | HD1 |
| MT2 (photo, 10 K) | 1/2 | tetragonal | 2.019 38 | 1.994 90 | first | 2 | 0.93 | 0.4 | HD2 |
| | | | | | second | 12 | 0.32 | 0.2 | |
| MT3 (photo, 10 K) | 1/2 | tetragonal | 2.019 38 | 1.994 90 | not observed | | | | HD2 with exchange interaction |
| B3 (40 K) | 1/2 | tetragonal ($D_{2d}$) | 2.015 90 | 2.005 10 | first | 2 | 1.36 | 0.76 | Ref. [39] tetrainterstitial Si |
| | | | | | second | 4 | 0.54 | 0.5 | ($I_4$) in $p$-type Si |
| | | | | | third | 8 | 0.29 | 0.2 | |

froze into a doubly occupied state ($S = 0$). Therefore, we consider HD2 as a double donor; HD2 always favors either a doubly occupied state or an empty state. Thus, HD2 has a negative-$U$ nature. Under photoexcitation, HD2 captures a photoexcited carrier, generating a self-trapped carrier with a HD2, which is EPR-active as the MT2/3 EPR signal. Such behaviors resemble those of thermal double donors (the NL10 EPR center) in Si [47,48].

Contrarily, HD1 is regarded as a normal positive-$U$ donor such as the P donor; a frozen state is EPR-active (MT1 EPR signal) in the dark. The MT1 EPR signal decreased in the dark below 15 K [Fig. 3(a)] as the MT1 center was converted into its doubly occupied state ($S = 0$). We speculate that part of the CEs was used to generate doubly occupied states of HD1s. Under photoexcitation where the CR signal recovers [Fig. 5(b)], the HD1s become EPR-active again by capturing a photoexcited carrier.

One may wonder why the sum of the MT1, MT2, and MT3 spin densities is approximately equal to the total concentration of HDs (Table I), although each HD2 emitted *two* electrons.

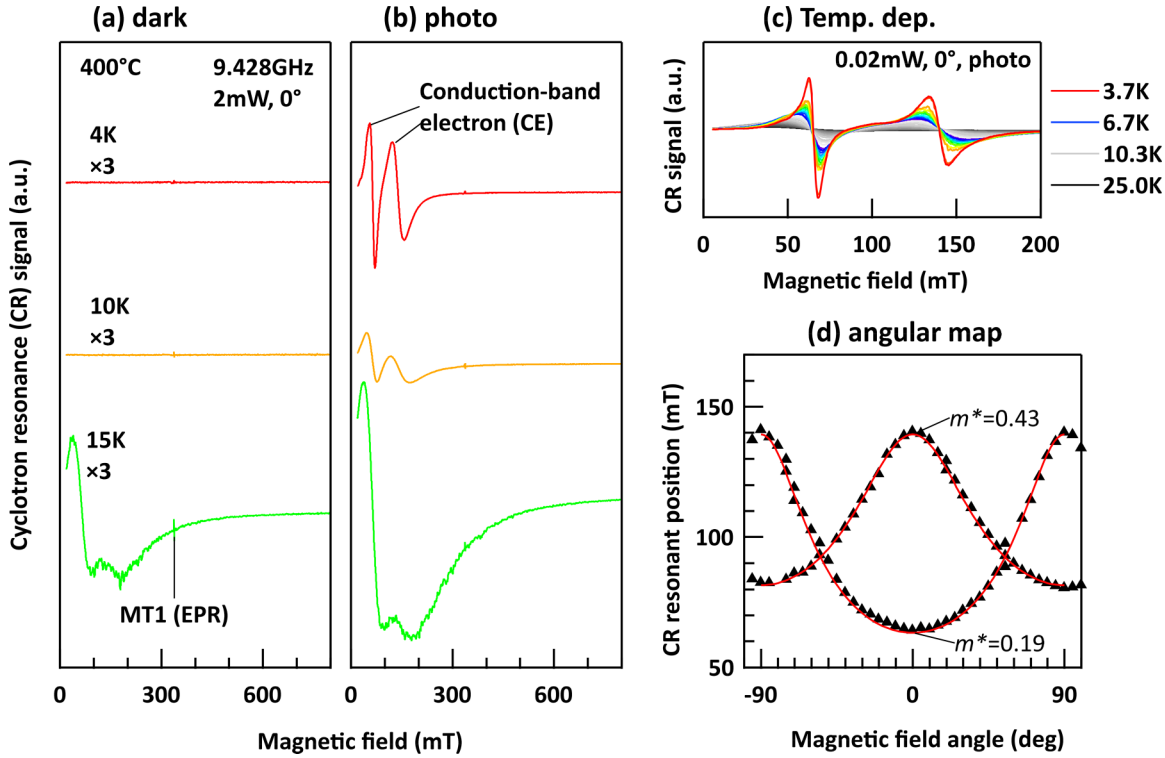


FIG. 5. CR spectra of the 400 °C sample measured (a) in the dark and (b) under photoexcitation. (c) Temperature dependence of the CR signal examined at a lower microwave power (but decreased CR signal intensities). (d) Angular map of the CR signal which is excellently fitted with the known effective masses of conduction-band electrons in Si [46]. Cyclotron resonant field (position) is calculated by $m^* m_0 / 2\pi e \nu$, where $m^*$ is the electron effective mass, $m_0$ is the electron rest mass, $e$ is the electron charge, and $\nu$ is the microwave frequency [46]. The angular dependence of the cyclotron resonant field was calculated using Eq. (38) in Ref. [46].

TABLE III. Comparison between EPR and CR results. The statuses of HD1, HD2, and conduction-band electrons (CEs) are explained.

| Signal (origin) | Dark, 15 K | Dark, below 15 K | Photoexcitation |
|---|---|---|---|
| MT1 (HD1) | Detected<br>HD1 stays in a single-occupied state ($S = 1/2$). | Decreased<br>Part of HD1 receives an electron and is converted into a double-occupied state ($S = 0$). | Detected<br>HD1 captures a photoexcited carrier. |
| MT2/3 (HD2) | Not detected<br>HD2 emits double electrons to the conduction band and stays in an empty state ($S = 0$). | Not detected<br>HD2 receives double electrons and is stabilized to a double-occupied state ($S = 0$). Part of HD2 remains in an empty state. | Detected<br>HD2 captures a photoexcited carrier, and a self-trapped carrier generates MT2/3 signals. |
| CR (CE) | Detected<br>CEs are emitted from HD2s. | Not detected<br>CEs return to HD2s and partly to HD1s. | Detected<br>Photoexcited CEs are generated. |

To satisfy the above equality, we have to assume the charge transfer between the HD2s; i.e., one HD2 moves its electron to another HD2, resulting in a pair of an empty state and a doubly occupied state of two HD2s. This behavior is expected for a negative-$U$ center. Then, only the doubly occupied state of an HD2 emits two electrons. The close pair is favorable for HD2, because of the all-time presence of the exchange-narrowing MT3 signal. Therefore, it is reasonable to expect the charge transfer between HD2s.

### D. Hyperfine interactions of HDs

Assuming that an HD comprises an intrinsic defect and hydrogen atom(s), we can expect HF interactions of $^{29}$Si nuclear spin(s) (nuclear spin $I = 1/2$, natural abundance = 4.7%) and $^{1}$H nuclear spin(s) ($I = 1/2$, natural abundance = 99.9%). $^{1}$H HF interactions are easily detectable owing to a doublet HF splitting in EPR spectrum; however, such a splitting was never found in the MT1, MT2, and MT3 centers. The incorporation of hydrogen into HDs has been evidenced by infrared-absorption experiments with a deuterium substitution [30,32]. We can therefore conclude that the $^{1}$H HF splitting widths should be significantly smaller than the observed EPR signal width ($\ll 0.2$ mT). $^{1}$H HF splitting is reduced because of two factors: the spatial separation of an unpaired-electron wave function from $^{1}$H nuclear spin(s), and the widely spreading wave function of the donor electron that significantly weakens any HF interactions [48].

The core structure of the HDs can be revealed via their $^{29}$Si HF interactions. In Fig. 6(a), we find a $^{29}$Si doublet HF structure in the low-field-side MT2 signal (0.93 mT splitting; black arrows). Additionally, this signal is the superposition of three peaks caused by another $^{29}$Si HF splitting (red arrows). Contrarily, MT1 and MT3 do not reveal any HF structures, as indicated by Figs. 6(a) and 6(b) and by other EPR data.

The $^{29}$Si HF doublet structures of the low-field-side MT2 signal can be well fitted by the "first shell" (two equivalent Si atoms) and the "second shell" (12 equivalent Si atoms) of $^{29}$Si HF structures [see Fig. 7(a)].These HF doublets became unclear in the high-field-side MT2 signal, however, they apparently convoluted $^{29}$Si HF structures as simulated in Fig. 7(b). By rotating the magnetic field in the $(0\bar{1}1)$ plane, we found that these $^{29}$Si HF doublets show a tetragonal symmetry [Fig. 7(c)]. The determined $^{29}$Si HF parameters are summarized in Table II. The $^{29}$Si HF tensor and the symmetry of MT2 and the B3 EPR center [39] are similar, although the B3 signal enabled us to deconvolute the second shell (12 atoms) into two groups (four and eight atoms). Figure 7(d) shows the angular pattern of the B3 center using the spin-Hamiltonian (SH) parameters in Table II, which resembles that of MT2. In fact, the B3 center was found to be a type of implantation damage evolving after 300–500 °C postimplantation annealing [39]. This formation behavior exactly coincides with that of the HDs in the present samples. Therefore, we conclude that the MT2 and MT3 centers (originated from HD2) were closely related to the B3 ($I_4$) centers [39]. Given the

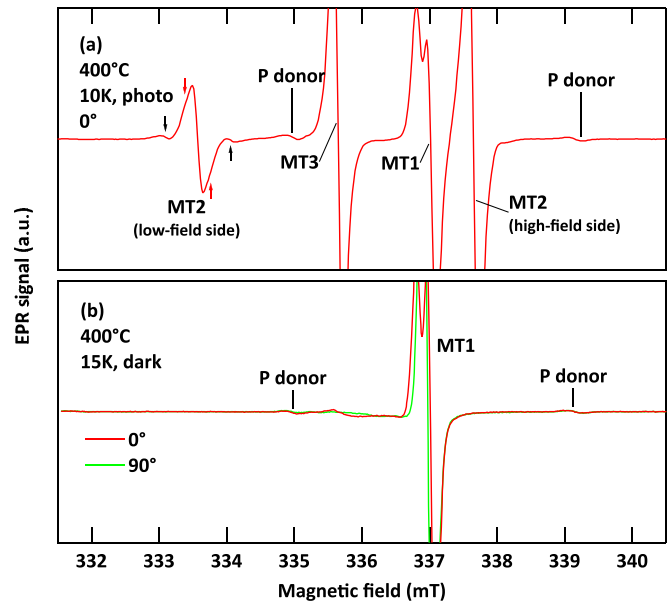


FIG. 6. HF interactions in HD EPR spectra, measured (a) under photoexcitation and (b) in the dark. In (a), the arrows indicate the $^{29}$Si HF doublets of MT2. MT3 is a single Lorentzian-like peak without any HF structures, suggesting that MT3 is an exchange-narrowing signal. In (b), MT1 (for 0° and 90°) does not exhibit any HF structures (see the right half side of MT1 signal). Its left half side is obscured by weak interference signal(s) probably owing to weak CR signal(s).

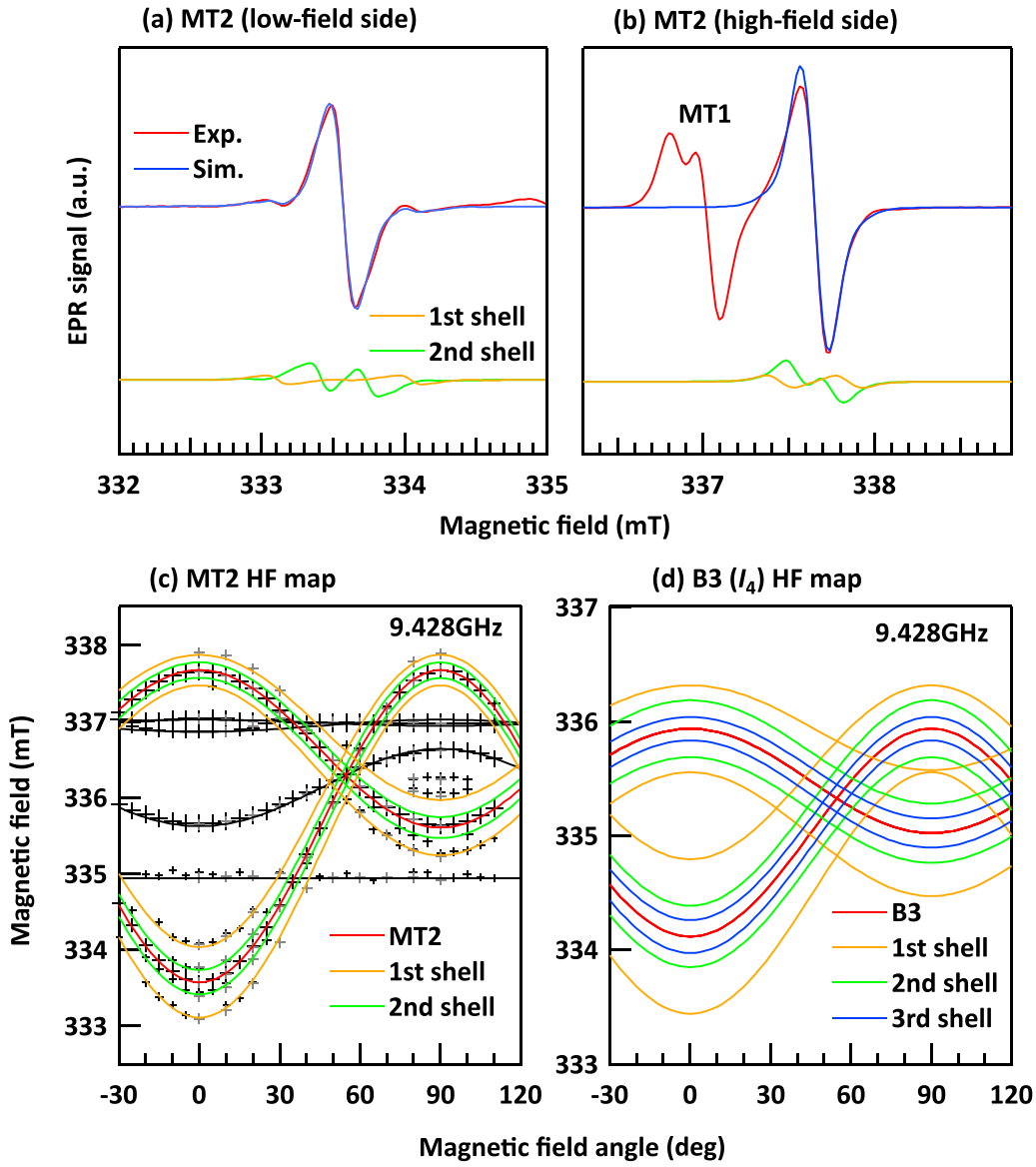


FIG. 7. $^{29}$Si HF interactions of MT2. (a) Low-field-side and (b) high-field-side MT2 signals simulated by two sets of $^{29}$Si HF doublets (first shell: orange; second shell: green).$^{29}$Si HF splitting in (a) and (b) corresponds to $A_{//}$ and $A_{\perp}$ components, respectively (see Table II). In (b), we focused on a spectral simulation using the right half side of MT2, because of the overlapped MT1 signal in the left half side of MT2. Angular maps of $^{29}$Si HF interactions for (c) the MT2 and (d) the B3 centers. In (c), the symbols (black and gray) are the individual experimental data measured at 10 K under photoexcitation. The solid lines plot the simulation data using the SH parameters ($g$ and $^{29}$Si HF tensors) shown in Table II.

similar formation condition and same tetragonal symmetry, we speculate that another HD (HD1) is also a type of B3-related center.

## IV. DISCUSSION ON MICROSCOPIC HD MODEL

Hydrogen and certain defects were inevitable in the formation of HDs [22–38], and the concentration of HDs increased linearly with the proton-irradiation dose, independent of the primary impurities (i.e., carbon and oxygen) concentrations in Si [43]. Moreover, the annealing kinetics of HDs (observed at 260–500 °C) indicated similarities with that of an interstitial silicon cluster [44]. Previous results suggest that HDs are intrinsic defects coupled with hydrogen and correlated with interstitial silicon [44].

Gorelkinskii *et al.* [23–25] and Tokmoldin *et al.* [32,33] investigated proton-irradiation-induced donors and suggested that the interstitial Si clusters participate in the donor formation process. Among the interstitial Si clusters, triinterstitial silicon ($I_3$) and tetrainterstitial silicon ($I_4$) are known to be thermally stable in the temperature range 250–500 °C (250–350 °C for $I_3$, and 300–500 °C for $I_4$ [39,44]), where the HDs (HD1 and HD2) are just observable. Jones and Carvalho *et al.* [49–51] demonstrated the trigonal $I_3$ [Fig. 8(a)] and tetragonal $I_4$ models [Fig. 8(b)] using DFT calculations. Furthermore, the $I_4$ center with $D_{2d}$ symmetry (tetragonal symmetry with the ⟨100⟩ symmetry axis) was identified to

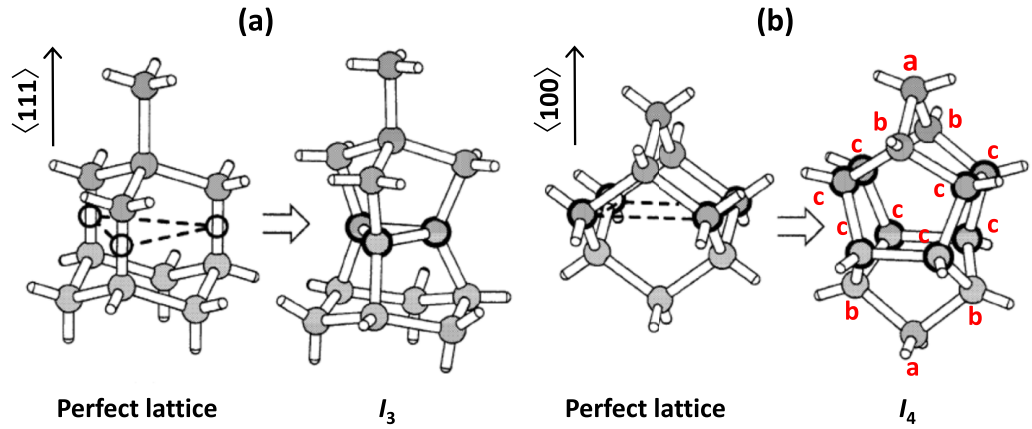


FIG. 8. (a) Trigonal triinterstitial and (b) tetragonal tetrainterstitial Si [49]. The left part of each image shows the perfect Si lattice before the insertion of the extra interstitial Si atoms. In (a), the $I_3$ center is constructed by placing three interstitial Si atoms at the bond center of adjacent ⟨111⟩ bonds. In (b), the $I_4$ center is constructed by replacing four neighboring Si atoms on the (100) plane with four ⟨100⟩ split interstitial pairs; (a)–(c) denote the Si shells described in the text.

be the origin of the B3 EPR center [39,49]. Likewise, the B5 EPR center with $C_{3v}$ symmetry (trigonal symmetry with ⟨111⟩ symmetry axis) was assigned to the $I_3$ center [39,49]. Additionally, the possible donor levels of the $I_3$ and $I_4$ centers were demonstrated near the valence band edge: $E_v + 0.19$ eV for $I_3$ and $E_v + 0.29$ eV for $I_4$, i.e., the $I_3$ and $I_4$ centers are deep donors [51].

A possible scenario in which two types of HDs correspond to the sole $I_3$- and $I_4$-based donors could be invoked. However, the experimentally verified symmetry presented here rules out the incorporation of the $I_3$ center with $C_{3v}$ symmetry into the HDs. Alternatively, we here propose a model in which both HDs (HD1 and HD2) are based on the $I_4$ center. The observed first shell of the $^{29}$Si HF structures arises from two Si atoms, "*a*," along a ⟨100⟩ axis, resulting in a strongly anisotropic tetragonal symmetry of the MT2 center. Twelve Si atoms of the second shell of the MT2 center are also assignable to Si atoms "*b*" and "*c*" [see Fig. 8(b)].

The difference between HD1 and HD2 may be attributed to different numbers of incorporated hydrogen atoms and/or their different bonding to $I_4$. HD2 likely involves more hydrogen atoms because HD2 forms at a higher temperature than HD1. For example, HD1 may be transformed into HD2 by capturing additional hydrogen atom(s) when elevating the annealing temperature from 400 °C to 500 °C. The electron-nuclear double resonance (ENDOR) study for weak $^1$H HF interactions remains a future work to verify this speculation.

For MT1 (HD1), we found a conduction-electron-like $g$ value and absence of any HF signatures, which is characteristic of a widely delocalized wave function of a donor electron and in contrast with the MT2/3 (HD2). For MT2/3, we also imagine a similar delocalized donor state, because we believe that HD1 and HD2 are the same $I_4$-based donors. A self-trapped carrier should be accompanied by a structural relaxation and a lowered symmetry as compared to the original structure before carriers are trapped. Because the MT2/3 centers are interpreted as a self-trapped carrier with an HD2, they may enhance their tetragonal symmetry, resulting in the observed strong $g$ anisotropy, which was stronger than that of the original $I_4$ center (see Table II). Nevertheless, comparing the $^{29}$Si HF interactions between MT2 and B3, we confirm that the HD electron is more delocalized than the $I_4$ center. Using Table II, a wave-function density of an unpaired electron, $\eta^2$, at the first shell (Si atoms *a*) [39] can be estimated: $\eta^2 = 4.8\%$ per Si atom ($3s$ orbital $0.4\% + 3p$ orbital $4.4\%$) for MT2, which is decreased from $\eta^2 = 5.6\%$ per Si atom for the B3 ($I_4$) center.

Based on the $I_4$ model, the MT2 center (HD2) consists of three types of Si atoms [*a* to *c* in Fig. 9(a)] and a 4.8% wave-function density of unpaired electrons at each Si atom *a*. However, the $^1$H HF interactions were completely hidden within the signal width (0.2 mT) in the EPR results.

Herein, we discuss the possible hydrogen site in the structure of HDs and reason(s) of the absence of a resolved $^1$H HF interactions. In Si, only a few cases in which $^1$H HF interactions have been clearly detected are known [see Figs. 9(b) and 9(c)]. Figure 9(b) shows an interstitial form of a hydrogen atom, $H_{BC}$ (the AA9 EPR center), which was also produced by proton irradiation but at 77 K with a much heavier dose ($10^{15}$ cm$^{-2}$) than that of the present study [2]. This center showed a strongly anisotropic $^1$H HF splitting of 0.22 to 1.1 mT [2]. If such a bond-centered hydrogen was formed near Si atoms *a* or *b* of HD2 [Fig. 9(a)], we could have detected $^1$H HF splitting. The neutral $V + H$ center [Fig. 9(c)] shows an anisotropic $^1$H HF splitting of 0.11 to 0.30 mT [19]. This anisotropic HF interaction arises from a dipolar interaction between an electron spin and a $^1$H nuclear spin that are separated by 0.28 nm in a monovacancy [19]. As this HF splitting is also within the experimentally detectable range, Si-H bonds for Si atoms *a* or *b* may be ruled out. Namely, Si atoms *c* may be the most probable site for the Si-H form or bond-centered hydrogen incorporation. We also speculate that the Si-H bond formation at Si atoms *c* may destabilize the structure of the $I_4$ center. Therefore, a hydrogen interstitial form or an intercalation form seems to be the most acceptable, as the core of HDs ($I_4$) is surrounded by a relatively large "cage" formed by eight Si atoms *c*. When such forms are introduced somewhere in Si atoms *c*, their $^1$H HF interactions may be significantly weakened. In Table IV, we further check

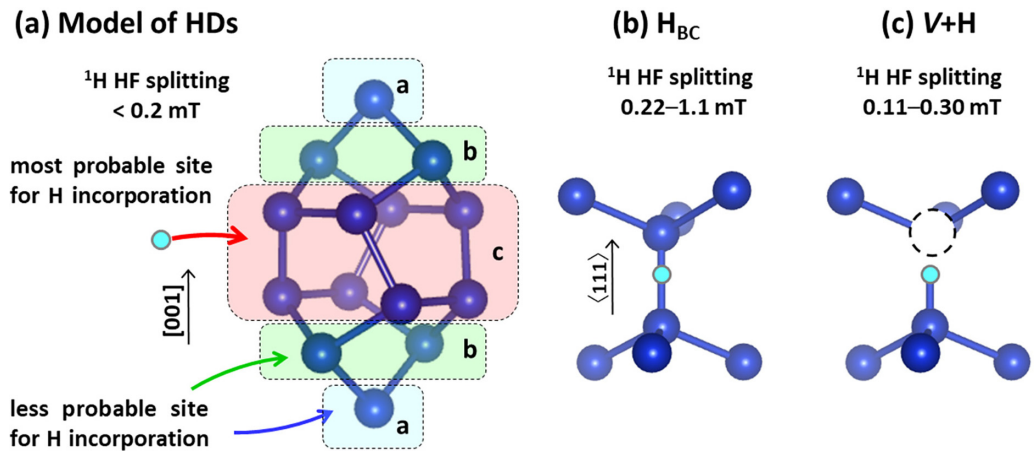


FIG. 9. Hydrogen interactions of paramagnetic centers in Si. The hydrogen and Si atoms are indicated by light blue and blue colors, respectively. (a) Possible site for hydrogen incorporation in HDs. Three areas for H incorporations are indicated by blue, green, and red, which correspond to equivalent Si atoms *a*, *b*, and *c*, respectively. The red area and surrounding cage formed by the Si atoms are the most probable site for the hydrogen incorporation. $^1$H HF interactions have been detected in Si in (b) a bond-centered hydrogen atom (AA9 center, $S = 1/2$ with trigonal or $C_{3v}$ symmetry) [2], (c) a monovacancy coupled with a hydrogen atom ($S = 1/2$ with monoclinic-*I* symmetry) [19]. In (c), monovacancy is depicted by a dotted circle.

$^1$H HF interactions quantitatively. First, assuming an effective mass (EM) donor (typically P in silicon) centered at the Si atom *a* in Fig. 9(a), its wave function yields isotropic $^1$H HF splitting as shown by $A_{\text{isotropic}}$ in Table IV, when a $^1$H nuclear spin is located at each position, respectively. All the estimated values (1.7–2.2 mT) are within an easily detectable range in the present EPR experiments. Therefore, we suggest that HDs have rather different wave function from the EM donors. For example, we infer that its wave function is not spherical and may have a node in the vicinity of the hydrogen location. We also calculated the dipolar interactions of a $^1$H nuclear spin, $A_{\text{dipole}}$. Judging from this calculation, we conclude again that the *c* site or inside the cage are only possible candidates for the location of hydrogen.

At present, the exact position of hydrogen atoms and how hydrogen atoms create shallow-donor levels of $I_4 + H_n$ is not clear ($n$ is unknown). This should be studied in the future, e.g., via ENDOR measurements and first-principles calculations based on the $I_4$-based donor.

Last, HDs are industrially useful for *n*-doping in Si devices. The present study revealed a fundamental limit of their thermal stability to 550 °C, which is the anneal-out temperature of the $I_4$ center [39,44].

## V. SUMMARY

We studied hydrogen-related donors (HDs) in Si, which are important defects for device applications and for an important unresolved issue in semiconductor science: how hydrogen behaves as a donor. We reported EPR signals (MT1, MT2, and MT3) in proton-irradiated FZ-Si annealed at 400 °C and 500 °C. Through a direct comparison of concentrations measured using SR profiling and EPR spectroscopy, the three signals were attributed to the HDs: MT1 to HD1 with lower thermal stability and MT2/3 to HD2 with higher thermal stability. Based on the full angular dependency of the MT1 EPR signal, its *g* tensor showed a conduction-electron-like *g* value but tetragonal symmetry around the ⟨100⟩ axis; no HF interaction was observed with any nuclear spins. HD1 behaved as a normal shallow donor, similar to the P donor. Contrarily, HD2 revealed a double-donor behavior (negative-*U* behavior). The MT2/3 EPR signals of HD2 were only detectable under photoexcitation as a self-trapped carrier with an HD2. MT2 presented a strongly anisotropic *g* tensor with a tetragonal symmetry around the ⟨100⟩ axis. MT3 was considered as an exchange-narrowing signal of MT2. For HD2, we demonstrated the preferential formation of close pairs and the preferential charge transfer in the pairs. We could not find $^1$H

TABLE IV. Estimated hyperfine coupling constants between an EM donor electron and a hydrogen nuclear spin. The distance *R* correspond to the separation between the Si atom *a* and expected hydrogen sites in the unrelaxed $I_4$ structure shown in Fig. 9(a). The calculation procedures are described in the Appendix.

| Position of $^1$H nuclear spin | Distance *R* (nm) | $A_{\text{isotropic}}$ (mT) | $A_{\text{dipole}}$ (mT) | Remarks |
|---|---|---|---|---|
| Si atom *a* site | 0 | 10.4 | | |
| Si atom *b* site | 0.23 | 2.2 | 0.2 | first neighboring site |
| Si atom *c* site | 0.34 | 1.6 | 0.1 | second neighboring site |
| Center in the cage | 0.36 | 1.7 | 0.1 | |

HF interactions in every EPR center and hence concluded that their $^{1}$H HF interactions should be much smaller than 0.2 mT (signal widths). For MT2, the $^{29}$Si HF interactions were successfully detected and assigned to the first (two Si atoms) and second shells (12 Si atoms) of the $I_4$ (tetrainterstitial cluster) center. Originally, the B3 EPR center has been identified as the $I_4$ center [39]. This center was considered an implantation damage center that grew after annealing at temperatures of 300–500 °C [39], similar to the case of the present study, and exhibited characteristic $^{29}$Si HF interactions similar to those of MT2. Therefore, we proposed a microscopic model for an unidentified structural unit to be $I_4$ or the B3 center. Namely, the HDs consist of an $I_4$ core + hydrogen atom(s). Further studies to verify the incorporation of hydrogen into the HDs are underway using techniques such as ENDOR spectroscopy and first-principles calculations.

## ACKNOWLEDGMENTS

A.K. is grateful to J. Ito (SHI-ATEX Co., Ltd) and S. Takemoto (Melco Semiconductor Engineering Corp.) for their assistance with the proton-irradiation experiments and spreading resistance profiling measurements, respectively.

## APPENDIX

In Table IV, we estimated the isotropic and dipolar hyperfine interactions using the following theories. According to Ref. [52], the following isotropic hyperfine interaction $A_{\rm iso}(r)$ of EM donors (As, P, and Sb in silicon) was given in Eq. (42):

$$A_{\rm iso}(r) = \frac{8\pi}{3}\,\mu_{\rm B}\,\mu_{\rm N}\,g\,g_{\rm N}\,\eta\,|F(r)|^2,$$

where $r$ is the distance from the origin of the wave function, $\mu_{\rm B}$ is the Bohr magneton, $\mu_{\rm N}$ is the nuclear magneton, $g$ is the electron $g$ factor, $g_{\rm N}$ is the nuclear $g$ factor, $\eta$ is a constant (they used the value $\eta = 178$ reported in Ref. [53]), and $F(r)$ is the envelop function (1$s$-hydrgogenlike wave function) of an EM shallow donor, which is approximated following the dual-exponentials function given in Eq. (48) of Ref. [52],

$$F(r) = 0.850\,(\pi 15^3)^{-1/2}\,e^{-r/15\ \text{Å}} + 0.211\,(\pi 5^3)^{-1/2}\,e^{-r/5\ \text{Å}}.$$

Considering that the experimentally established isotropic hyperfine interaction of the P donor is $A^{\rm P}_{\rm iso}\ (r=0) = 4.195$ mT in silicon, we calculated the strength of isotropic hyperfine coupling of H atom separated with the distance $R$ from an EM shallow donor,

$$A^{\rm H}_{\rm iso}(R) = A^{\rm P}_{\rm iso}(0)\,\frac{|F(R)|^2}{|F(0)|^2}\,\frac{g_{\rm N}(^1\text{H atom})}{g_{\rm N}(^{31}\text{P atom})}.$$

We also calculated the strength of the dipolar hyperfine interaction, $A_{\rm dipole}(r)$, within the point-dipole approximation, according to Ref. [54],

$$A_{\rm dipole} = \frac{\mu_0}{4\pi}\,\frac{\mu_{\rm B}\,\mu_{\rm N}\,g\,g_{\rm N}}{h\,R^3},$$

where we used 2.79 and 1.13 for the nuclear $g$ factor of H and P atoms and 2.0 for the electron $g$ factor, respectively.


[1] S. J. Pearton, J. W. Corbett, and T. S. Shi, Appl. Phys. A **43**, 153 (1987).
[2] Y. V. Gorelkinskii and N. N. Nevinnyi, Phys. B (Amsterdam, Neth.) **170**, 155 (1991).
[3] S. J. Pearton, J. W. Corbett, and M. Stavola, *Hydrogen in Crystalline Semiconductors* (Springer-Verlag, Heidelberg, 1992).
[4] *Hydrogen in Semiconductors*, edited by J. J. Pankove, and N. M. Johnson (Academic, Boston, 1991).
[5] *Hydrogen in Compound Semiconductors*, edited by S. J. Pearton (Trans Tech, Aedermannsdorf, 1994).
[6] R. F. Kiefl and T. L. Estele, Phys. B (Amsterdam, Neth.) **170**, 33 (1991).
[7] N. M. Johnson and C. Herring, Phys. Rev. B **45**, 11379 (1992).
[8] S. K. Estreicher, M. Stavola, and J. Weber, in *Silicon, Germanium, and their Alloys* (CRC, Boca Raton, 2014), Chap. 7.
[9] A. R. Peaker, V. P. Markevich, and L. Dobaczewski, in *Defects in Microelectronic Materials and Devices* (CRC, Boca Raton, 2008), Chap. 2.
[10] K. J. Chang and D. J. Chadi, Phys. Rev. B **40**, 11644 (1989).
[11] C. G. Van de Walle, P. J. H. Denteneer, Y. Bar-Yam, and S. T. Pantelides, Phys. Rev. B **39**, 10791 (1989).
[12] G. D. Watkins and J. R. Troxell, Phys. Rev. Lett. **44**, 593 (1980).
[13] C. G. Van de Walle, Phys. Rev. B **49**, 4579 (1994).
[14] A. W. R. Leitch, V. Alex, and J. Weber, Phys. Rev. Lett. **81**, 421 (1998).
[15] R. E. Pritchard, M. J. Ashwin, J. H. Tucker, and R. C. Newman, Phys. Rev. B **57**, R15048(R) (1998).
[16] J. D. Holbech, B. Bech Nielsen, R. Jones, P. Sitch, and S. Öberg, Phys. Rev. Lett. **71**, 875 (1993).
[17] P. J. H. Denteneer, C. G. Van de Walle, and S. T. Pantelides, Phys. Rev. B **41**, 3885 (1990).
[18] B. B. Nielsen, L. Hoffmann, and M. Budde, Mater. Sci. Eng. B **36**, 259 (1996).
[19] B. B. Nielsen, P. Johannesen, P. Stallinga, K. B. Nielsen, and J. R. Byberg, Phys. Rev. Lett. **79**, 1507 (1997).
[20] P. Hazdra and J. Vobecky, Solid State Phenom. **69–70**, 545 (1999).
[21] N. M. Johnson, F. A. Ponce, R. A. Street, and R. J. Nemanich, Phys. Rev. B **35**, 4166 (1987).
[22] Y. Zohta, Y. Ohmura, and M. Kanazawa, Jpn. J. Appl. Phys. **10**, 532 (1971).
[23] Y. V. Gorelkinskii, N. N. Nevinnyi, and V. A. Botvin, Radiat. Eff. **49**, 161 (1980).
[24] Y. V. Gorelkinskii and N. N. Nevinnyi, Nucl. Instrum. Methods Phys. Res. **209–210**, 677 (1983).
[25] Y. V. Gorelkinskii, N. N. Nevinnyi, and K. A. Abdullin, J. Appl. Phys. **84**, 4847 (1998).
[26] K. Nakamura, S. Nishizawa, and A. Furukawa, IEEE Trans. Electron Devices **67**, 2437 (2020).
[27] M. Nemoto, T. Yoshimura, and H. Nakazawa, Appl. Phys. Express **1**, 051404 (2008).
[28] R. Job, J. G. Laven, F. J. Nidernostheide, H. J. Schulze, H. Schulze, and W. Schustereder, Phys. Status. Solidi A **209**, 1940 (2012).

[29] J. G. Laven, H. J. Schulze, V. Häublein, F. J. Niedernostheide, H. Schulze, H. Ryssel, and L. Frey, Phys. Status Solidi C **8**, 697 (2011).
[30] J. Hartung and J. Weber, Phys. Rev. B **48**, 14161 (1993).
[31] H. Hatakeyama and M. Suezawa, J. Appl. Phys. **82**, 4945 (1997).
[32] S. Z. Tokmoldin and B. N. Mukashev, Phys. Status Solidi B **210**, 307 (1998).
[33] S. Z. Tokmoldin, A. T. Issova, K. A. Abdullin, and B. N. Mukashev, Phys. B (Amsterdam, Neth.) **376-377**, 185 (2006).
[34] J. G. Laven, R. Job, H. -J. Schulze, F. -J. Niedernostheide, W. Schustereder, and L. Frey, ECS J. Solid State Sci. Technol. **2**, 389 (2013).
[35] E. Ntsoenzok, P. Desgardin, M. Saillard, J. Vernois, and J. F. Barbot, J. Appl. Phys. **79**, 8274 (1996).
[36] V. P. Markevich, M. Suezawa, K. Sumino, and L. I. Murin, J. Appl. Phys. **76**, 7347 (1994).
[37] J. Coutinho, R. Jones, P. R. Briddon, S. Öberg, L. I. Murin, V. P. Markevich, and J. L. Lindström, Phys. Rev. B **65**, 014109 (2001).
[38] C. P. Ewels, R. Jones, S. Öberg, J. Miro, and P. Deák, Phys. Rev. Lett. **77**, 865 (1996).
[39] D. Pierreux and A. Stesmans, Phys. Rev. B **71**, 115204 (2005).
[40] J. F. Ziegler, J. P. Biersack, and U. Littmark, in *Stopping and Ranges of Ions in Matter*, Vol. 1 (Pergamon, New York, 1984), Chap. 3.
[41] W. R. Thurber, R. L. Mattis, Y. M. Liu, and J. J. Filliben, J. Electrochem. Soc. **127**, 1807 (1980).
[42] C. A. J. Ammerlaan, O. Madelung, U. Rössler, and M. Schulz, in *Landort-Börnstein New Series, Group III, Part 41A2α, Impurities and defects in group IV elements, IV-IV and III-V compounds* (Springer-Verlag Berlin, Heidelberg, 2002), pp. 244–308.
[43] A. Kiyoi, N. Kawabata, K. Nakamura, and Y. Fujiwara, J. Appl. Phys. **130**, 115704 (2021).
[44] A. Kiyoi, N. Kawabata, K. Nakamura, and Y. Fujiwara, J. Appl. Phys. **131**, 125702 (2022).
[45] G. Feher and E. A. Gere, Phys. Rev. **114**, 1245 (1959).
[46] G. Dresselhaus, A. F. Kip, and C. Kittle, Phys. Rev. **98**, 368 (1955).
[47] S. H. Muller, M. Sprenger, E. G. Sieverts, and C. A. J. Ammerlaan, Solid State Commun. **25**, 987 (1978).
[48] Y. V. Martynov, T. Gregorkiewicz, and C. A. J. Ammerlaan, Phys. Rev. Lett. **74**, 2030 (1995).
[49] R. Jones, T. A. G. Eberlein, N. Pinho, B. J. Coomer, J. P. Goss, P. R. Briddon, and S. Öberg, Nucl. Instrum. Methods Phys. Res. B **186**, 10 (2002).
[50] B. J. Coomer, J. P. Goss, R. Jones, S. Öberg, and P. R. Briddon, J. Phys.: Condens. Matter **13**, L1 (2001).
[51] A. Carvalho, R. Jones, J. Coutinho, and P. R. Briddon, Phys. Rev. B **72**, 155208 (2005).
[52] J. L. Ivey and R. L. Mieher, Phys. Rev. B **11**, 822 (1975).
[53] D. K. Wilson, Phys. Rev. **134**, A265 (1964).
[54] A. Schweiger and G. Jeschke, *Principles of Pulse Electron Paramagnetic Resonance* (Oxford University Press, Oxford, 2001).